

RFDM: Residual Flow Diffusion Model for Efficient Causal Video Editing

Mohammadreza Salehi^{*†}, Mehdi Noroozi^{*}, Luca Morreale,
Ruchika Chavhan, Malcolm Chadwick, Alberto Gil Ramos, Abhinav Mehrotra
Samsung AI Research

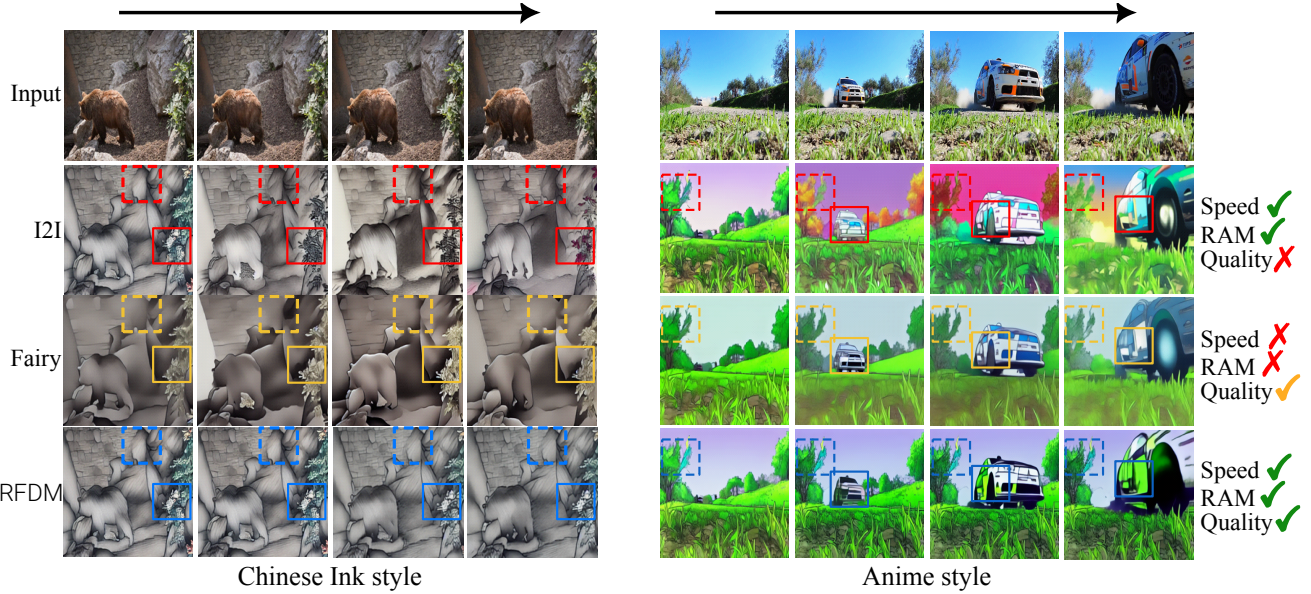


Figure 1. **Video style transfer.** Editing video style requires understanding of motion and style across frames. Naive Image-to-Image(I2I) models generate inconsistent video frames. Fairy smoothens the result, trading computational cost to achieve lower jittering and inconsistency. RFDM results in the most consistent edit, while being computationally similar to the per-frame baseline (I2I). The video is taken from the DAVIS.

Abstract

Instructional video editing applies edits to an input video using only text prompts, enabling intuitive natural-language control. Despite the rapid progress, most methods still require fixed-length inputs and substantial compute. Meanwhile, autoregressive video generation enables efficient variable-length synthesis, yet remains under-explored for video editing. We introduce a causal, efficient video editing model that edits variable-length videos frame by frame. For efficiency, we start from a 2D image-to-image (I2I) diffusion model and adapt it to video-to-video (V2V) editing by conditioning the edit at time step t on the model’s prediction at $t - 1$. To leverage videos’ temporal redundancy, we propose a new I2I diffusion forward process formulation that encourages the model to predict the residual between the target output and the previous prediction. We call this Residual Flow Diffusion Model (RFDM), which focuses the denoising

process on changes between consecutive frames. Moreover, we propose a new benchmark that better ranks state-of-the-art methods for editing tasks. Trained on paired video data for global/local style transfer and object removal, RFDM surpasses I2I-based methods and competes with fully spatiotemporal (3D) V2V models, while matching the compute of image models and scaling independently of input video length. More content can be found in [RFDM page](#).

1. Introduction

Instructional video editing aims to edit an input video using only a natural-language prompt (e.g., “remove the object” or “turn the object red”), eliminating extra conditioning signals such as object masks [36, 47]. Recent methods have made strong progress by proposing different ways of coupling video generative models with text encoders or large language models [1, 34, 41, 52] or adapting an image-based model for video editing [19, 28, 32, 43]. However, all these approaches rely on non-causal temporal mechanisms

^{*}Equal contribution.

[†]Work done during the internship at Samsung.

that require fixed-length inputs and demand high computational cost, which is constraining in applications such as video streaming [4, 27] or their deployment on resource-constrained devices such as cell phones [20].

Meanwhile, autoregressive video generation [10, 37, 53] has recently been recognized as a solution to variable-length input requirements and can be relatively efficient due to causal attention. However, such methods remain under-explored for video editing and still require further efficiency to operate in real time or on resource-constrained devices. We therefore propose a *causal* and *efficient* framework that edits videos autoregressively, frame by frame. For efficiency, we use 2D image-to-image (I2I) diffusion models as the backbone and make them causal by (i) conditioning each prediction at time step t on the previous-frame prediction as an input, which adds no extra compute, and (ii) Leveraging videos' temporal redundancy, we propose a novel forward diffusion process that shifts the sampling-noise mean toward the previous prediction, turning current frame prediction into a residual prediction between consecutive frames. As shown in Figure 1 (I2I vs. RFDM), applying an I2I model independently to each frame yields inconsistent edits due to diffusion stochasticity or input frame variability; in contrast, our method produces consistent results on the same backbone, with no additional computational overhead.

Finally, we show that existing benchmarks that use metrics based on CLIP textual similarity between edited videos and prompts are insufficient to measure the faithfulness of edits, resulting in sub-optimal method rankings; we therefore introduce a new benchmark with new metrics and provide extensive qualitative and quantitative evaluations. We call our model **RFDM** (Residual Flow Diffusion Model) and train it on the recently released *Señorita* [56] dataset. The evaluations on 3 benchmarks show that RFDM beats all models that are based on a similar 2D backbone and competes with models on a 3D backbone across three prompt categories: global style transfer, local style transfer, and object removal. In summary:

- We propose a causal video editing model built on I2I backbones, solving the fixed-length input requirement while adding no overhead than an I2I model.
- We adapt the I2I backbone to videos by (i) conditioning each time step on the previous prediction, and (ii) introducing a novel diffusion forward process that encourages predicting inter-frame residuals rather than full frames.
- We present a new benchmark and accompanying metrics, and evaluate RFDM extensively on it and two additional benchmarks. RFDM achieves stronger faithfulness, competitive performance, and orders-of-magnitude lower latency compared to state-of-the-art.

2. Related works

We categorize video editing models into text-guided and other modality-guided approaches. Text-guided models edit videos solely based on textual prompts, enabling editing through natural language. In contrast, models in the latter group require additional inputs such as object masks [15, 18], optical flow [8, 12, 38], or audio cues [26]. In the following, we focus on text-guided methods, as they share the same setup as ours.

Zero/few-shot methods. These methods leverage pre-trained text-to-image (T2I), image-to-image (I2I), or text-to-video (T2V) models and adapt them for video editing tasks in a zero-shot or few-shot manner [2, 6, 13, 28, 31, 32, 34, 40, 41, 43, 45, 48]. T2I and I2I methods have similar computational costs and are substantially cheaper than T2V models. Zero-shot methods, such as VideoDirector [41], build upon pre-trained T2V models and steer the DDIM inversion process to achieve temporally consistent edits guided by text prompts. Similar ideas have been explored in FateZero [31] and VideoGrain [48], which adapt T2I backbones for video editing. Another line of zero-shot approaches enforces temporal coherence by aligning spatially similar features across frames, either through feature merging as in VidToMe [28] or spatio-temporal cross-attention as in Fairy [43]. In contrast, few-shot methods finetune the backbone to personalize edits using a small set of videos or images, as demonstrated in Tune-A-Video [45]. While such methods are effective when the full video is accessible during inference, they cannot generate videos autoregressively—i.e., editing each frame based only on preceding frames—and either require fine-tuning the backbone for each new video or demand high computational costs due to heavy spatio-temporal attention across all frame tokens. RFDM, similar to Fairy and VidToMe, builds on a T2I backbone; however, it introduces no additional computational overhead beyond that of an image model, requires no per-video finetuning, and operates in an autoregressive manner.

Training-based methods. Existing approaches often depend on massive datasets and large video-based backbones [17, 35, 50], which are difficult to access and reproduce. To address this, some methods [5] train on synthetically generated data and adapt image-based models to videos by incorporating non-autoregressive spatio-temporal attention mechanisms, which increase computational cost with video length and perform less effectively on real-world videos. In contrast, RFDM is trained on the *Señorita* dataset [56]—the first large-scale, open-source video editing dataset constructed from real-world videos—and employs a novel autoregressive conditioning scheme that maintains the efficiency of image-based models without adding computational overhead.

3. Method

In this section, we discuss our proposed Residual Flow Diffusion Model (RFDM) for video editing. Our objective is to adapt an image-to-image (I2I) model to an autoregressive video-to-video (V2V) model. More precisely, given a series of input video frames denoted by $X = \{x_t | t = 0, \dots, T\}$, and an instruction prompt p . We aim to train a diffusion model that edits the video auto-regressively frame-by-frame, producing a set of output frames denoted by $Y = \{y_t^0 | t = 0, \dots, T\}$. To perform the edit consistently over the video, RFDM is conditioned on the previous prediction, \hat{y}_{t-1} .

In the following, we first present an overview of diffusion models for instruction-based image editing, then we discuss our proposed RFDM that adapts the I2I model to V2V. We denote the diffusion time-step by s and the video temporal frames by t .

3.1. Diffusion Models for Image Editing.

Given a triplet $\{x, p, y^0\}$, the task of image editing involves modifying the input image, x , based on the instruction prompt, p , to closely match the target image y^0 . Therefore, posing the task as a conditional image generation. Seminal work, Instruct-pix2pix [1] poses it with the following diffusion forward process:

$$\begin{aligned} q(y^s | y^0) &= \mathcal{N}(\alpha^s y^0, (\sigma^s)^2 I); \quad s \in [0, 1] \\ y^s &= \alpha^s y^0 + \sigma^s \epsilon; \quad \epsilon \sim \mathcal{N}(0, I). \end{aligned} \quad (1)$$

Where α^s, σ^s define the noise schedule, such that the log signal-to-noise ratio, $\lambda^s = \log[\frac{\alpha^s}{\sigma^s}]$, decreases with s monotonically.

The parameters of the denoising distribution, θ , is learned via a denoising function through the following objective function¹:

$$\arg \min_{\theta} \|\hat{y}_{\theta}(y^s, x, p, \lambda_s) - y^0\| \quad (2)$$

Classifier Free Guidance (CFG) enables high-fidelity image sampling during inference with prompt adherence [11], resulting in a procedure that combines three different calls of the conditional and unconditional denoising model.

3.2. Residual Flow Diffusion Models

The main challenge of converting an I2I to V2V lies in handling the temporal inconsistency across frames. Indeed, naively applying a I2I model independently per-frame generates inconsistent motion across frames. Our primary objective is to improve temporal consistency via conditioning

¹This objective function can be optimized with other parameterizations such as ϵ , etc. [21]. We use x parameterization throughout this paper without losing generalizability.

on its own prediction. That is, for a given frame at time t , the model is conditioned on its own prediction at $t - 1$, and is supervised during the training through consistent ground truth.

Frame prediction. A straightforward approach involves deploying a similar forward process as Eq. 1 but conditioning only the denoising model. More precisely, the forward process for the frame at time t has the following form:

$$\begin{aligned} q(y_t^s | y_t^0) &= \mathcal{N}(\alpha^s y_t^0, (\sigma^s)^2 I); \quad s \in [0, 1] \\ y_t^s &= \alpha^s y_t^0 + \sigma^s \epsilon; \quad \epsilon \sim \mathcal{N}(0, I). \end{aligned} \quad (3)$$

Additionally, the denoising process is conditioned on the previous prediction \hat{y}_{t-1} ², resulting in the following objective function:

$$\arg \min_{\theta} \|\hat{y}_{\theta}(y_t^s, \hat{y}_{t-1}, x_t, p, \lambda_s) - y_t^0\|;$$

where $t \in [0, T]$ and $\hat{y}_{-1} = 0$.

Residual Flow Prediction. Inspired by [54] on image inverse problems, we modify our forward process such that instead of generating the entire frame from pure noise, it rephrases the problem in the light residual generation between the target frames. In particular, we denote the temporal residual m_t^0 between the target and past prediction as $m_t^0 = \hat{y}_{t-1} - y_t^0$. We use it to rephrase the forward process as follows:

$$\begin{aligned} q(y_t^s | y_t^0, \hat{y}_{t-1}) &= \mathcal{N}(\alpha^s y_t^0 + \sigma^s \hat{y}_{t-1}, (\sigma^s)^2 I) \\ &= \mathcal{N}(\gamma^s y_t^0 + \sigma^s m_t^0, (\sigma^s)^2 I) \end{aligned} \quad (4)$$

where $\gamma^s = \sqrt{1 - (\sigma^s)^2} + \sigma^s$.³ The forward process in Eq. 4 forms a Markov chain that transits the target at frame t to the noisy version of the previous prediction through the temporal residual between them. This is equivalent to shifting the mean of the sampling noise in the diffusion process:

$$\begin{aligned} y_t^s &= \alpha^s y_t^0 + \sigma^s \hat{y}_{t-1} + \sigma^s \epsilon; \quad \epsilon \sim \mathcal{N}(0, I) \\ &= \alpha^s y_t^0 + \sigma^s \hat{\epsilon}; \quad \hat{\epsilon} \sim \mathcal{N}(\hat{y}_{t-1}, I) \end{aligned} \quad (5)$$

Denoising process. The denoising process estimates the conditional posterior distribution $p_{\theta}(y_t | y_t^s, \hat{y}_{t-1}, x_t, p)$ for which we train a denoising function $\hat{y}_{\theta}(y_t^s, \hat{y}_{t-1}, x_t, p, \lambda_s)$ parametrized by a neural network in the following objective function:

²We denote the past predictions with \hat{y} because there are multiple options during the training, which we discuss later.

³Note that in flow models, $\gamma^s = 1 \forall s$. In the case of diffusion models, it is close to 1 most of the time.

Algorithm 1 RFDM training

Input: Input video clip $x_t = \{x_0, \dots, x_T\}$
Input: Output video clip $y_t = \{y_0^0, \dots, y_T^0\}$
Input: instruction prompt p
Input: noise schedule $\alpha^s, \sigma^s, \lambda^s$ \triangleright for $s \in [0, 1]$
Input: initialization θ \triangleright from text-to-image
Sample K sorted indices $\{k_0, \dots, k_K\} \in [0, T]$
 $\hat{y}_{-1} \leftarrow 0$
 $\mathcal{L} \leftarrow 0$
for $i \in [0, \dots, K]$ **do**
 $t \leftarrow k_i$
 $s \sim \mathcal{U}(0, 1)$
 $\epsilon \sim \mathcal{N}(0, I)$
 $y_t^s \leftarrow \alpha^s y_t^0 + \sigma^s \hat{y}_{t-1} + \sigma^s \epsilon$
 $\hat{y}_t \leftarrow \hat{y}_\theta(y_t^s, x_t, \hat{y}_{t-1}, p)$
 $\mathcal{L} += \text{MSE}(\hat{y}_t, y_t^0)$ \triangleright Apply the loss on all frames.
end for
Update θ via backpacking through \mathcal{L} .

$$\arg \min_{\theta} \|\hat{y}_\theta(y_t^s, \hat{y}_{t-1}, x_t, p, \lambda_s) - y_t^0\|. \quad (6)$$

The advantage of Eq. 5 to 3 lies in the supervision signal, which we elaborate in the following.

An efficient way for the network to optimize the denoising model is to split the pixels into two groups. I) The areas that are already edited in \hat{y}_{t-1} , such as background or a moving object that is present in both frames; the model needs to just shift them to y_t . II) The new areas, where the model needs to edit them based on x_t and the instruction prompt. The forward process in Eq. 5 explicitly enforces this strategy, where the residual is explicitly embedded in the noisy input.

Sampling. During the sampling, we start with editing the first frame from the pure noise using the DDIM sampler. To edit the next frames, we start from a noise shifted by the previous frame prediction and repeat this process until the last frame. We use CFG to edit each frame as proposed in [1].

Handling the exposure bias. Exposure bias refers to the discrepancy between the way an autoregressive model is used during the training and inference [14], resulting in degraded video quality over time during the inference in the case of video generation. Handling exposure bias translates to the choices for \hat{y}_{t-1} in our notation, where, despite the inference time that we only have access to the model's inference prediction distribution, there are multiple choices to sample \hat{y}_{t-1} during the training. A straightforward choice is to use the ground truth frames, i.e. y_{t-1}^0 , which is known as Teacher Forcing (TF) [42]. However, as we ablate in the experiments section, the model trained with TF degrades quickly during inference. One reason could be the reliance

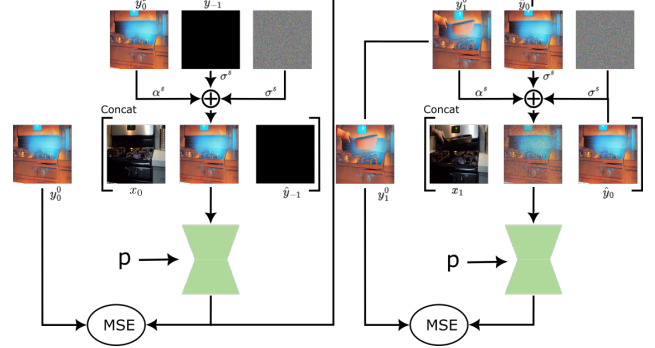


Figure 2. **Training.** We obtain the noisy input(y_t^s) at time frame t by fusing current frame(x_t), previous prediction(\hat{y}_{t-1}), and noise through a noise scheduler via Eq. 5. For a given video clip, we edit the first frame, where the noisy input is obtained by adding noise to the target; where the first target is $\hat{y}_{-1} = 0$. Thereafter, the output on the previous frame is used as input (\hat{y}_1). The amount of noise, i.e. α^s, σ^s , is sampled independently for each frame. This figure shows a scenario where the amount of noise is low in the first frame, i.e. $\alpha^s \rightarrow 1$, and high in the second frame, i.e. $\alpha^s \rightarrow 0$. In the latter, where the amount of noise is high, y_t^s is close to the noisy \hat{y}_{t-1} . In addition to y_t^s , the denoising model takes x_t and \hat{y}_{t-1} as extra inputs via concatenation and the instruction prompt via cross attention.

on clean y_{t-1}^0 during the training, which suffers from a shift between the model's imperfect prediction distribution during the inference. To close the gap between the training and inference distribution of \hat{y}_{t-1} , we follow Diffusion Forcing (DF) [3]. That is, we sample different random noise levels for different frames during the training to generate the noisy inputs, and use the denoising model prediction at frame $t-1$ to sample \hat{y}_{t-1} . As a result, the past observations are still clean, but they are sampled from the model's training distribution, which is closer to the model's inference distribution compared with the ground truth in TF. During the inference, we edit each frame in a fully sequential manner, and use the past frame's clean output to condition next frame editing. The training and inference processes are illustrated in detail in Algorithm 1, Figure 2 and Algorithm 2, Figure 3 respectively.

4. Experiments

4.1. Experimental setup

We train RFDM on SD1.5 [33] (RFDM1.5) and SD3.5 (M) [7] (RFDM3.5) as our backbones. For training, we utilize the recently introduced Señorita-2M [56] dataset, which contains 2 million paired videos covering five instructional video editing tasks: global style transfer, local style transfer, object removal, object addition, and object swap. As the dataset lacks predefined train, validation, and test splits, we introduce a fixed random split of 80%, 15%, and 5%, respectively, for consistent training, evaluation, and test. We split the data between train (80%), validation (5%), and test (15%). RFDM is trained on 8 A100 GPUs for

Algorithm 2 RFDM inference

Input: Input video clip $X = \{x_0, \dots, x_T\}$
Input: instruction prompt p
Input: noise schedule $\alpha^s, \sigma^s, \lambda^s$ \triangleright for $s \in [0, 1]$
Input: ω_x, ω_{xp} \triangleright cfg coefficients
Output: Output video clip $\bar{Y} \leftarrow \{\}$
 $\hat{y}_{-1} \leftarrow 0$ \triangleright previous frame perdition
for $t \in 0, \dots, T$ **do**
 $\epsilon \sim \mathcal{N}(0, I)$
 $\bar{y}_t^s \leftarrow \hat{y}_{t-1} + \epsilon$ \triangleright initial noisy input
for $s \in [S, \dots, 1]$ **do**
 $y_{pred}^\emptyset \leftarrow \hat{y}_\theta(\bar{y}_t^s, \hat{y}_{t-1}, \emptyset, \emptyset, \alpha^s, \sigma^s)$
 $y_{pred}^x \leftarrow \hat{y}_\theta(\bar{y}_t^s, \hat{y}_{t-1}, x_t, \emptyset, \alpha^s, \sigma^s)$
 $y_{pred}^{xp} \leftarrow \hat{y}_\theta(\bar{y}_t^s, \hat{y}_{t-1}, x_t, p, \alpha^s, \sigma^s)$
 $y_{pred} \leftarrow y_{pred}^\emptyset + \omega_x(y_{pred}^x - y_{pred}^\emptyset)$
 $\quad + \omega_{xp}(y_{pred}^{xp} - y_{pred}^x)$
 $\bar{y}_t^{s-1} \leftarrow \text{DDIM}(y_{pred}, \bar{y}_t^s, \alpha^s, \sigma^s)$
end for
 $\hat{y}_{t-1} \leftarrow \bar{y}_t^0$
 Add \bar{y}_t^0 to \bar{Y}
end for
 return \bar{Y}

45k steps with a batch size of 8, gradient accumulation of 2, a learning rate of $1e^{-4}$ using the Adam optimizer [22].

4.2. Evaluation benchmarks and metrics

Benchmarks. We evaluate RFDM on three benchmarks: TGVE [5], TGVE+ [35] and Señorita [56]. TGVE and TGVE+ capture prompt alignment based on detailed captions provided for each (input, output) video pair when ground-truth data is absent. This provides a useful proxy for prompt alignment and temporal coherence without ground truth; however, its reliance on text limits evaluation of two core aspects: *temporal consistency*, *i.e.*, preserving edits across frames, and *faithfulness*, *i.e.*, leaving unrelated regions unchanged. Therefore, as a third complementary benchmark, we leverage the ground-truth data in the Señorita dataset and introduce the *Señorita Benchmark*, which enables direct comparison between edited outputs and reference videos on the test split of Señorita. This benchmark overcomes both limitations by enabling direct evaluation of temporal consistency and faithfulness to the input content. We report performance on the test set across three editing tasks: global style transfer, local style transfer, and object removal, which together provide a comprehensive assessment of each method’s versatility on real-world videos.

Metrics. For TGVE and TGVE+, we report the metrics proposed for the benchmark, including CLIPFrame [46], PickScore [23], and ViCLIP_{out} [35]. For Señorita, we eval-

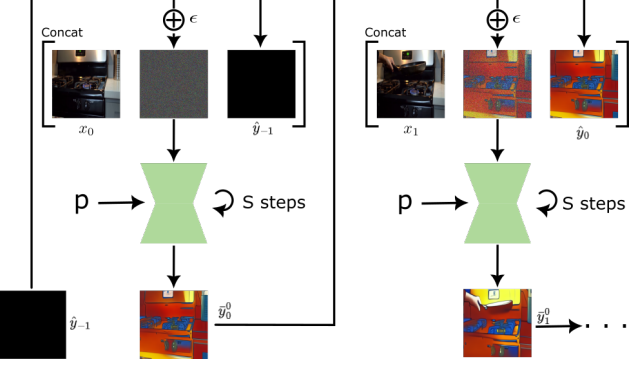


Figure 3. **Inference illustration.** We edit the frame at time t by starting from the noisy previous frame (\hat{y}_{t-1}), and applying the denoising steps. The first frame, where $y_{-1} = 0$, is edited in an I2I manner, starting from pure noise. In each denoising step, the current input frame(x_t) and the clean previous prediction(\hat{y}_{t-1}) are given to the model as extra input via concatenation to the noisy input. The instruction prompt is provided via cross-attention.

uate four complementary protocols that collectively assess the quality of generated videos from different perspectives: (i) Warping Error [25] quantifies *temporal consistency* by measuring optical-flow-based deformation between consecutive frames. (ii) ViDreamSim, which we introduce, extends DreamSim [9] to videos by comparing each output frame with its ground-truth counterpart, capturing *faithfulness*. (iii) Directional Visual Similarity (DVS) [29] computes the average similarity of direction vectors between the input–output and input–ground-truth frames using CLIP’s visual encoder, assessing whether the visual transformation aligns with the intended change in a text-free manner. (iv) Error Accumulation, which we also introduce in this work, measures the drift commonly observed [39, 51] in autoregressive models by quantifying how the distribution of later frames deviates from that of the first output frame. (v) MLLM-as-a-Judge prompts GPT-4o [16] to rate how well the edited video fulfills the user instruction, providing a holistic score from 1 to 10.

We formally define ViDreamSim and Error Accumulation as follows:

$$\text{ViDREAMSIM} = \frac{1}{T} \sum_{t=1}^T d(\bar{y}_t^0, y_t^0), \quad (7)$$

$$\text{ERRACCU} = \frac{1}{T-1} \sum_{t=1}^T d(\bar{y}_t^0, \bar{y}_0^0), \quad (8)$$

where \bar{y}_t^0 and y_t^0 denote the output and ground-truth frames at time t , respectively, $d(\cdot, \cdot)$ represents a perceptual distance metric such as DreamSim, and T is the number of frames. Qualitative illustrations of error accumulation and temporal consistency, along with details of the MLLM-as-a-Judge protocol, are provided in the supplementary material.

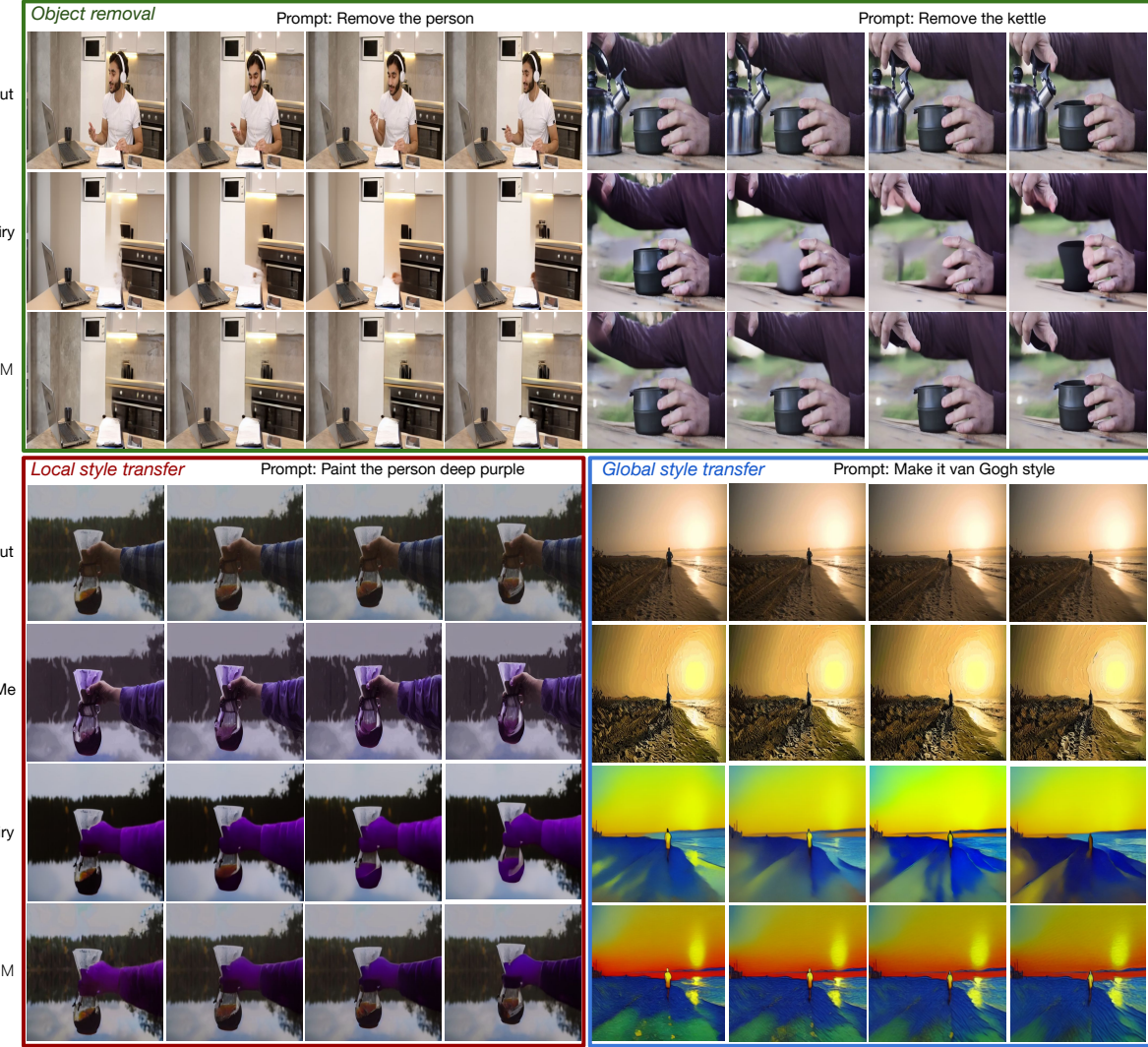


Figure 4. **Qualitative results.** We compare RFDM with Fairy and VidToMe on Señorita benchmark across object removal (green), local style transfer (red), and global style transfer (blue). VidToMe is shown only for the style-transfer tasks as it is not designed for object removal. Compared to Fairy, RFDM yields more consistent and higher-fidelity outputs, especially in object removal where Fairy often leaves noticeable artifacts or alters irrelevant regions. VidToMe produces temporally consistent videos but deviates more from the ground truth than both RFDM and Fairy.

Baseline methods. We compare RFDM against two categories of methods: those built upon fully spatio-temporal (3D) V2V backbones, such as EVE [35], and those based on I2I backbones (2D), such as Fairy [43] and VidToMe [28]. To ensure a fair comparison, for the latter group, which employs the same backbone as ours, we report results using both their original SD1.5 model and our pretrained variant. We use the official repository for VidToMe [28] and reproduce Fairy [43] ourselves, as its implementation is not publicly available.

4.3. Video editing results

TGVE, TGVE+ and Señorita benchmarks. We compare RFDM against state-of-the-art nobaselines in both edit-

ing quality and computational efficiency in Table 1. On TGVE and TGVE+, RFDM3.5 leads in 4 of 6 metrics across the two benchmarks and performs competitively with proprietary V2V models such as EVE, despite relying on a much more efficient I2I backbone. In efficiency, RFDM3.5 matches Fairy’s latency while using $\sim 13\times$ less RAM, and reduces latency by $\sim 4\times$ compared to other baselines. Even the smaller RFDM1.5 remains competitive with I2I state-of-the-art methods such as TokenFlow and RAVE on TGVE/TGVE+, while being $\sim 12\text{--}16\times$ faster and requiring $\sim 4\text{--}5\times$ less RAM. Notably, all RFDM variants achieve the highest CLIPFrame score, suggesting strong temporal consistency, driven by conditioning on \hat{y}_{t-1} (the previous prediction) and predicting a residual flow that updates only

Table 1. **Video editing results on TGVE, TGVE+ and Señorita.** TGVE and TGVE+ results are taken from [35, 55] except for RAVE and TokenFlow, which we report. Señorita results are averaged across style transfer, local style transfer, and object removal tasks. TempCon denotes temporal consistency. * marks methods using our pretrained UNet as the backbone. Latency and RAM are reported for generating 16 frames by us on an A100 GPU. Our models are highlighted in blue, and proprietary (closed source and data) models are shown in gray.

Method	Causal	TGVE			TGVE+			Señorita test set				16-frame generation	
		ViCLIP _{out} ↑	PickScore↑	CLIPFrame↑	ViCLIP _{out} ↑	PickScore↑	CLIPFrame↑	DVS↑	MLLM-Judge↑	ViDreamSim↓	TempCon↓	Lat.(s)↓	RAM(GB)↓
Fairy [43]	✗	0.208	19.8	0.933	0.197	19.81	0.933	0.32	2.87	0.63	0.043	<u>13</u>	77
Fairy*	✗	—	—	—	—	—	—	0.40	3.98	0.29	0.042	<u>13</u>	77
AnyV2V [24]	✗	0.230	19.70	0.919	0.227	19.80	0.919	—	—	—	—	100	15
STDF [49]	✗	0.226	20.40	0.933	0.227	20.60	0.933	—	—	—	—	300	20
TokenFlow [32]	✗	0.257	20.58	0.943	0.231	19.88	0.943	0.29	3.23	0.48	0.010	128	11
RAVE [19]	✗	0.254	20.35	0.936	0.250	20.03	0.932	0.34	3.54	0.42	0.017	92	9
InsV2V [5]	✗	<u>0.262</u>	20.76	0.911	0.236	20.37	0.925	—	—	—	—	53	8
VidToMe [28]	✗	—	—	—	—	—	—	0.32	3.10	0.46	0.007	86	9
VidToMe*	✗	—	—	—	—	—	—	0.37	1.77	0.59	0.014	86	9
EVE [35]	✗	0.262	20.76	0.922	0.251	20.88	0.926	—	—	—	—	—	—
RFDM1.5	✓	0.260	20.29	<u>0.949</u>	<u>0.236</u>	19.33	<u>0.964</u>	<u>0.43</u>	<u>6.60</u>	<u>0.23</u>	0.010	8	<u>2</u>
RFDM3.5	✓	0.284	<u>20.66</u>	0.965	0.250	<u>20.52</u>	0.970	0.48	7.57	0.20	0.008	<u>13</u>	6

changed regions. Compared to EVE, RFDM3.5 attains slightly lower PickScore, which can be explained by EVE’s substantially larger 3D backbone (4.4B vs. 2.5B parameters for SD3.5) and its much larger training set (34M vs. 2M videos in Señorita). Since EVE is closed-source, we cannot directly measure or report its computational cost.

On Señorita, we compare against prior methods, which use similar I2I backbones. As shown, both variants of RFDM consistently outperform all others, both with their original UNet and when re-trained with ours, across DVS, MLLM-Judge, and ViDreamSim, while maintaining comparable temporal consistency. The lower ViDreamSim and higher DVS scores show closer alignment with the ground truth, also confirmed by MLLM-Judge. The slightly lower temporal consistency compared to VidToMe stems from RFDM’s stronger faithfulness to the ground truth, whereas VidToMe produces smoother yet less accurate outputs. This underscores the advantage of the Señorita benchmark, as its use of ground-truth data enables more accurate and discriminative evaluation of model faithfulness and editing performance. More details in the supplementary material.

Qualitative results. We qualitatively illustrate the results in Figure 4 and Figure 5. As shown in Figure 4, RFDM produces cleaner edits in the object removal task, leaving fewer artifacts and consistently inpainting backgrounds. Likewise, for both local and global style transfer, it generates videos with the highest faithfulness and temporal consistency. For instance, Fairy fails to maintain faithfulness over time, turning both the liquid and the person pink, while VidToMe deviates from the ground truth from the very first frame. We illustrate the effect of applying multiple global style transfer prompts to the same video in Figure 5, demonstrating the method’s ability to generalize and produce diverse outputs from a single input. We provide an extensive qualitative evaluation in the supplementary material.

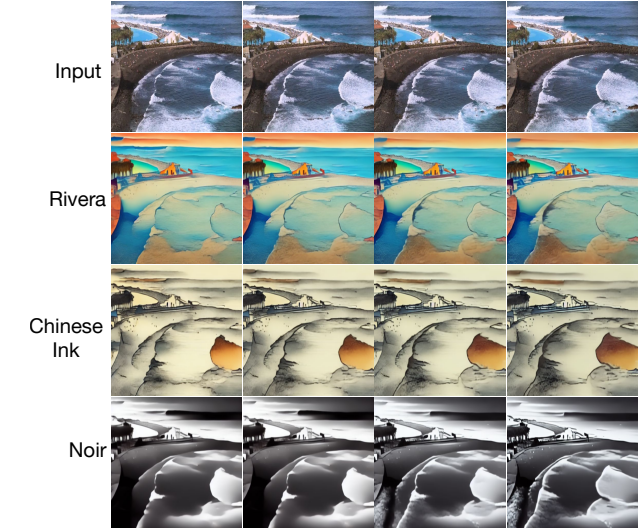


Figure 5. **Different styles generated by RFDM on Señorita.** RFDM produces consistent and faithful outputs across a wide range of styles and input videos.

4.4. Ablations

We conduct ablations on key parameters of RFDM using our smaller variant, SD1.5 backbone, and the Señorita validation set for global style transfer. The number of frames used in the autoregressive loss is fixed to 3 in all ablations, except in the ablation studying this parameter. Our objective is to identify configurations that yield high temporal consistency, low error accumulation, and strong faithfulness to the ground truth. We observe that temporal consistency and error accumulation are discriminative across all ablations except one, for which faithfulness must also be considered. Below, we discuss the impact of each parameter in detail.

Number of autoregressive frames. In Table 2a, we

Table 2. **Ablating the key parameters of, RFDM.** We report temporal consistency and error accumulation on the Señorita global style transfer validation set. \uparrow and \downarrow indicate that higher or lower values are better, respectively. The blue row, is our default setup.

(a) Autoregressive frames			(b) Input conditioning			(c) Forcing approach			
NUM.	TEMPCON \downarrow	ERRACCU \downarrow	INP.	TEMPCON \downarrow	ERRACCU \downarrow	METHOD	TEMPCON \downarrow	ERRACCU \downarrow	ViDREAMSIM \downarrow
0	0.068	0.21	x	0.027	0.14	Teacher	0.009	0.06	0.38
1	0.013	0.12	x, \hat{y}_{t-1}	0.009	0.07	Diffusion	0.009	0.07	0.35
3	0.009	0.07							
5	0.007	0.07							

(d) Key-frame update interval			(e) Grad propagation			(f) Prediction task formulation			(g) DAVIS Tracking		
Δ Frames	TEMPCON \downarrow	ERRACCU \downarrow	UNROLLING	TEMPCON \downarrow	ERRACCU \downarrow	NOISE	TEMPCON \downarrow	ERRACCU \downarrow	Prediction	J \uparrow	F \uparrow
0	0.018	0.04	No	0.011	0.10	Frame	0.009	0.09	Frame	33.3	24.9
1	0.008	0.16	Yes	0.009	0.07	Residual-Flow	0.009	0.07	Residual-Flow	50.6	36.4
3	0.009	0.07									
5	0.010	0.07									

show that increasing the number of autoregressive frames in the loss leads to improved temporal consistency and reduced error accumulation. This is because training over longer temporal contexts exposes the model to its own prediction errors, yielding a stronger supervision signal. Therefore, we use 5 autoregressive frames as the default.

Input conditioning. The previous prediction is already utilized in the sampling noise during the inference. We additionally provide the clean previous prediction, denoted by \hat{y}_{t-1} , as an extra input in each sampling step. We ablate the impact of this extra input in Table 2b, showing the importance of this extra input, which boosts the performance.

Forcing approach. Table 2c ablates the effect of teacher forcing versus our adapted diffusion forcing, including an additional metric to assess output faithfulness. As shown, both methods achieve comparable temporal consistency, while teacher forcing yields slightly lower error accumulation. However, it diverges more from the ground-truth distribution, making it less suitable for inference. Hence, we adopt diffusion forcing in our main experiments.

Key-frame update interval. Error accumulation tends to increase when \hat{y}_{t-1} is updated at every frame. To mitigate this, during inference we update it every Δ frames. As shown in Table 2d, setting $\Delta = 0$ means for a frame at time t , the first frame output is always used as \hat{y}_{t-1} , leading to very low accumulation error but high temporal inconsistency. Increasing Δ from 1 to 3 reduces the accumulation error by roughly 50% (from 0.16 to 0.07) while causing only a minor drop in temporal consistency (around 10%), after which the benefits plateau, we set $\Delta = 3$.

Grad propagation. We ablate the impact of unrolling [30] – allowing or blocking the gradient flow – in all autore-

gressive losses. As shown in Table 2e, unrolling improves performance, as the model benefits from richer supervision through gradient backpropagation across all autoregressive stages. We use unrolling in our main results.

Prediction task. We compare the impact of residual-flow prediction and frame prediction formulations in Table 2f. As shown, residual-flow prediction results in lower error accumulation, which we attribute to its improved tracking capability that naturally emerges from the residual-flow formulation. To validate this, we selected 10 videos from DAVIS and segmented the first-frame objects using Qwen-Image-Edit [44]. We then conditioned both models, frame and residual-flow prediction, on Qwen-Image-Edit’s output with the same prompt and measured their tracking performance. As shown in Table 2g, given the same first-frame output, the residual-flow model propagates edits more accurately across frames, demonstrating superior tracking ability.

5. Conclusion and Discussion

In this paper, we introduced RFDM, an autoregressive video editing model that adapts an image-to-image backbone through a novel autoregressive conditioning based on residual-flow prediction. Trained on large-scale real-world videos from the Señorita dataset, we extensively ablated across three key aspects: temporal consistency, error accumulation, and faithfulness, and evaluated on both the proposed Señorita benchmark and TGVE+. The results show that causal I2I models like RFDM achieve strong performance and efficiency, pointing to a promising direction for scalable video editing. *Limitations:* Despite an excellent trade-off between the performance and computational efficiency, RFDM’s drawback lies in its short temporal memory, required in motion-constrained edits such as changing the action of a video. A plausible solution could be deploying a KV caching mechanism, which we leave to future work.

RFDM: Residual Flow Diffusion Model for Efficient Causal Video Editing

Supplementary Material

6. Experiments

6.1. Señorita Benchmark Details

[Table 3](#) reports the full quantitative results on the Señorita benchmark for our method, along with Fairy [43] and VidToMe [28], including per-task breakdown. We report the average scores, whereas here we show the complete tables for global style transfer, local style transfer, and object removal.

Overall, both variants of RFDM consistently improve over prior work across the majority of metrics, while maintaining orders of magnitude lower computational cost as shown in the paper Table 1. In particular, RFDM3.5 attains higher or comparable scores in both temporal consistency and faithfulness metrics, which aligns with our design choices of residual flow prediction and autoregressive conditioning. For completeness, we also include the corresponding qualitative videos and error plots in the accompanying HTML visualization page (project page linked in the supplementary material).

7. More qualitative results

In addition to the figures shown in the main paper, we provide a larger set of qualitative examples (149 videos) in the html page provided with this supplementary material. We kindly encourage the reviewer to open the page for more comprehensive qualitative comparison.

7.1. Failure cases

We summarize common failure cases of RFDM, with more detailed explanations and video examples provided in the HTML page attached to the supplementary material. We encourage the reviewer to refer to the HTML visualization page for detailed explanations and examples.

7.2. Better than ground-truth

We also observe several cases where RFDM produces results that appear more natural than the provided ground truth. Since the Señorita dataset’s ground truth is generated through a multi-stage pipeline combining segmentation, inpainting, and tracking modules, it can occasionally contain artifacts, flickering, or imperfect boundaries. Benefiting from the strong spatial understanding of SD1.5 and the temporal stability introduced by our proposed framework, RFDM often yields smoother and more coherent outputs that correct such imperfections. We encourage the reviewer to refer to the HTML visualization page in the supplementary material for side-by-side video comparisons.

7.3. Visualization of ablation studies

We visualize what is measured in our ablation studies through **error accumulation** and **temporal consistency** in the attached HTML page. As shown, when $\Delta = 0$, error accumulation remains low but temporal consistency degrades over time. At $\Delta = 1$, temporal consistency improves, though accumulated error increases. The balance is achieved at $\Delta = 3$, where both metrics remain stable. We encourage the reviewer to refer to the HTML visualization page in the supplementary material for corresponding video examples and plots.

8. MLLM-as-a-Judge

To obtain a human-aligned and instruction-aware evaluation of video editing quality, we employ a multimodal LLM-based scoring mechanism, referred to as *MLLM-as-a-Judge*. This evaluator uses GPT-4o [16] to assess how well an edited video satisfies the user instruction while preserving the structure and semantics of the original content.

Evaluation protocol. For each video, we consider the input sequence x , the predicted edited video \bar{y}_t^0 , and the ground-truth edit y_t^0 . We uniformly sample K frames from each sequence to form triplets

$$(x_k, \bar{y}_k^0, y_k^0), \quad k = 1, \dots, K.$$

Each triplet is processed independently to obtain frame-level judgments.

Prompting the MLLM. We provide the multimodal LLM with three images—the original frame, the edited frame produced by the method, and the ground-truth edited frame—along with the editing instruction. The model is asked to judge, in a comparative manner, how well the candidate edit adheres to the instruction while maintaining the spatial layout and identity of the original scene.

We use the following fixed prompt template:

You are an expert judge for video editing quality. You are given: (1) the original frame, (2) a candidate edited frame, and (3) the ground-truth edited frame, along with the editing instruction: '{p}'. Rate how well the candidate frame follows the instruction while preserving the content, structure, and visual coherence of the original frame.

Table 3. Señorita results are averaged across style transfer, local style transfer, and object removal tasks. TempCon denotes temporal consistency. * marks methods using our pretrained SD1.5 UNet as the backbone.

Task	Method	DVS \uparrow	MLLM-JUDGE \uparrow	TEMPCON \downarrow	ViDREAMSIM \downarrow
Style transfer	Fairy [43]	0.49	2.5	0.045	0.77
	Fairy*	0.56	3.7	0.048	0.50
	VidToMe [28]	0.51	3.5	0.007	0.60
	VidToMe*	0.57	1.5	0.015	0.51
	RFDM1.5	<u>0.59</u>	<u>6.0</u>	0.007	<u>0.43</u>
	RFDM3.5	0.63	7.5	<u>0.008</u>	0.36
Local editing	Fairy [43]	0.21	3.0	0.037	0.65
	Fairy*	0.29	4.0	0.037	0.17
	VidToMe [28]	0.22	2.8	0.007	0.35
	VidToMe*	0.26	1.5	0.015	0.61
	RFDM1.5	<u>0.34</u>	<u>6.3</u>	0.012	<u>0.13</u>
	RFDM3.5	0.40	6.8	<u>0.010</u>	0.12
Object removal	Fairy [43]	0.26	3.1	0.046	0.46
	Fairy*	0.35	4.2	0.042	0.19
	VidToMe [28]	0.23	3.0	0.007	0.43
	VidToMe*	0.29	2.3	0.012	0.65
	RFDM1.5	<u>0.37</u>	<u>7.5</u>	0.011	<u>0.12</u>
	RFDM3.5	0.40	7.8	<u>0.010</u>	0.11

Return a single score from 1 to 10, where 1 means ‘‘much worse than the ground truth’’ and 10 means ‘‘better than the ground truth’’. Output only the number.

Score aggregation. For each frame k , the MLLM outputs a scalar score $s_k \in \{1, \dots, 10\}$. The video-level score is the average across sampled frames:

$$\text{MLLM-Judge}(x, \bar{y}^0, y^0) = \frac{1}{K} \sum_{k=1}^K s_k.$$

Finally, the dataset-level score for a method is obtained by averaging over all videos. A higher score indicates that the edited frames are judged to:

- more faithfully follow the user-provided editing instruction,
- better preserve the identity, geometry, and temporal cues of the input,
- exhibit stronger perceptual coherence compared to the ground-truth edit.

Because the evaluation explicitly incorporates instruction text and visual context, it captures aspects of editing quality

that traditional pixel- or feature-based metrics fail to measure.

The same protocol is used for all video-editing tasks considered in this work, including global style transfer, local style transfer, and object removal.

References

[1] Tim Brooks, Aleksander Holynski, and Alexei A Efros. Instructpix2pix: Learning to follow image editing instructions. In *Proceedings of the IEEE/CVF conference on computer vision and pattern recognition*, pages 18392–18402, 2023. 1, 3, 4

[2] Duygu Ceylan, Chun-Hao P Huang, and Niloy J Mitra. Pix2video: Video editing using image diffusion. In *Proceedings of the IEEE/CVF International Conference on Computer Vision*, pages 23206–23217, 2023. 2

[3] Boyuan Chen, Diego Martí Monsó, Yilun Du, Max Simchowitz, Russ Tedrake, and Vincent Sitzmann. Diffusion forcing: Next-token prediction meets full-sequence diffusion. *Advances in Neural Information Processing Systems*, 37:24081–24125, 2024. 4

[4] Feng Chen, Bohan Zhuang, and Qi Wu. Streaming video diffusion: Online video editing with diffusion models. In *2025 International Conference on Digital Image Computing: Techniques and Applications (DICTA)*, pages 1–9. IEEE, 2025. 2

[5] Jiaxin Cheng, Tianjun Xiao, and Tong He. Consistent video-to-video transfer using synthetic dataset. *arXiv preprint arXiv:2311.00213*, 2023. 2, 5, 7

[6] Yuren Cong, Mengmeng Xu, Christian Simon, Shoufa Chen, Jiawei Ren, Yanping Xie, Juan-Manuel Perez-Rua, Bodo Rosenhahn, Tao Xiang, and Sen He. Flatten: optical flow-guided attention for consistent text-to-video editing. *arXiv preprint arXiv:2310.05922*, 2023. 2

[7] Patrick Esser, Sumith Kulal, Andreas Blattmann, Rahim Entezari, Jonas Müller, Harry Saini, Yam Levi, Dominik Lorenz, Axel Sauer, Frederic Boesel, et al. Scaling rectified flow transformers for high-resolution image synthesis. In *Forty-first international conference on machine learning*, 2024. 4

[8] Ruoyu Feng, Wenming Weng, Yanhui Wang, Yuhui Yuan, Jianmin Bao, Chong Luo, Zhibo Chen, and Baining Guo. Ccredit: Creative and controllable video editing via diffusion models. In *Proceedings of the IEEE/CVF Conference on Computer Vision and Pattern Recognition*, pages 6712–6722, 2024. 2

[9] Stephanie Fu, Netanel Tamir, Shobhita Sundaram, Lucy Chai, Richard Zhang, Tali Dekel, and Phillip Isola. Dreamsim: Learning new dimensions of human visual similarity using synthetic data. *arXiv preprint arXiv:2306.09344*, 2023. 5

[10] Yuchao Gu, Weijia Mao, and Mike Zheng Shou. Long-context autoregressive video modeling with next-frame prediction. *arXiv preprint arXiv:2503.19325*, 2025. 2

[11] Jonathan Ho and Tim Salimans. Classifier-free diffusion guidance. *arXiv preprint arXiv:2207.12598*, 2022. 3

[12] Zhihao Hu and Dong Xu. Videocontrolnet: A motion-guided video-to-video translation framework by using diffusion model with controlnet. *arXiv preprint arXiv:2307.14073*, 2023. 2

[13] Chi-Pin Huang, Yen-Siang Wu, Hung-Kai Chung, Kai-Po Chang, Fu-En Yang, and Yu-Chiang Frank Wang. Videomage: Multi-subject and motion customization of text-to-video diffusion models. In *Proceedings of the Computer Vision and Pattern Recognition Conference*, pages 17603–17612, 2025. 2

[14] Xun Huang, Zhengqi Li, Guande He, Mingyuan Zhou, and Eli Shechtman. Self forcing: Bridging the train-test gap in autoregressive video diffusion. *arXiv preprint arXiv:2506.08009*, 2025. 4

[15] Yi Huang, Wei Xiong, He Zhang, Chaoqi Chen, Jianzhuang Liu, Mingfu Yan, and Shifeng Chen. Dive: Taming dino for subject-driven video editing. In *Proceedings of the IEEE/CVF International Conference on Computer Vision*, pages 16004–16014, 2025. 2

[16] Aaron Hurst, Adam Lerer, Adam P Goucher, Adam Perelman, Aditya Ramesh, Aidan Clark, AJ Ostrow, Akila Welihinda, Alan Hayes, Alec Radford, et al. Gpt-4o system card. *arXiv preprint arXiv:2410.21276*, 2024. 5, 1

[17] Zeyinzi Jiang, Zhen Han, Chaojie Mao, Jingfeng Zhang, Yulin Pan, and Yu Liu. Vace: All-in-one video creation and editing. *arXiv preprint arXiv:2503.07598*, 2025. 2

[18] Kumara Kahatapitiya, Adil Karjauv, Davide Abati, Fatih Porikli, Yuki M Asano, and Amirhossein Habibian. Object-centric diffusion for efficient video editing. In *European Conference on Computer Vision*, pages 91–108. Springer, 2024. 2

[19] Ozgur Kara, Bariscan Kurtkaya, Hidir Yesiltepe, James M Rehg, and Pinar Yanardag. Rave: Randomized noise shuffling for fast and consistent video editing with diffusion models. In *Proceedings of the IEEE/CVF Conference on Computer Vision and Pattern Recognition*, pages 6507–6516, 2024. 1, 7

[20] Animesh Karnewar, Denis Korzhenkov, Ioannis Lelekas, Adil Karjauv, Noor Fathima, Hanwen Xiong, Vancheeswaran Vaidyanathan, Will Zeng, Rafael Esteves, Tushar Singhal, et al. Neodragon: Mobile video generation using diffusion transformer. *arXiv preprint arXiv:2511.06055*, 2025. 2

[21] Diederik Kingma and Ruiqi Gao. Understanding diffusion objectives as the elbo with simple data augmentation. *Advances in Neural Information Processing Systems*, 36: 65484–65516, 2023. 3

[22] Diederik P Kingma. Adam: A method for stochastic optimization. *arXiv preprint arXiv:1412.6980*, 2014. 5

[23] Yuval Kirstain, Adam Polyak, Uriel Singer, Shahbuland Matiania, Joe Penna, and Omer Levy. Pick-a-pic: An open dataset of user preferences for text-to-image generation. *Advances in neural information processing systems*, 36:36652–36663, 2023. 5

[24] Max Ku, Cong Wei, Weiming Ren, Harry Yang, and Wenhui Chen. Any2v2: A tuning-free framework for any video-to-video editing tasks. *arXiv preprint arXiv:2403.14468*, 2024. 7

[25] Wei-Sheng Lai, Jia-Bin Huang, Oliver Wang, Eli Shechtman, Ersin Yumer, and Ming-Hsuan Yang. Learning blind video temporal consistency. In *Proceedings of the European conference on computer vision (ECCV)*, pages 170–185, 2018. 5

[26] Seung Hyun Lee, Sieun Kim, Innfern Yoo, Feng Yang, Donghyeon Cho, Youngseo Kim, Huiwen Chang, Jinkyu

Kim, and Sangpil Kim. Soundini: Sound-guided diffusion for natural video editing. *arXiv preprint arXiv:2304.06818*, 2023. 2

[27] Runjia Li, Moayed Haji-Ali, Ashkan Mirzaei, Chaoyang Wang, Arpit Sahni, Ivan Skorokhodov, Aliaksandr Siarohin, Tomas Jakab, Junlin Han, Sergey Tulyakov, et al. Egoedit: Dataset, real-time streaming model, and benchmark for egocentric video editing. *arXiv preprint arXiv:2512.06065*, 2025. 2

[28] Xirui Li, Chao Ma, Xiaokang Yang, and Ming-Hsuan Yang. Vidtome: Video token merging for zero-shot video editing. In *Proceedings of the IEEE/CVF Conference on Computer Vision and Pattern Recognition*, pages 7486–7495, 2024. 1, 2, 6, 7

[29] Mehdi Noroozi, Alberto Gil Ramos, Luca Morreale, Ruchika Chavhan, Malcolm Chadwick, Abhinav Mehrotra, and Sourav Bhattacharya. Guidance free image editing via explicit conditioning. *arXiv preprint arXiv:2503.17593*, 2025. 5

[30] Razvan Pascanu, Tomas Mikolov, and Yoshua Bengio. On the difficulty of training recurrent neural networks. In *International conference on machine learning*, pages 1310–1318. Pmlr, 2013. 8

[31] Chenyang Qi, Xiaodong Cun, Yong Zhang, Chenyang Lei, Xintao Wang, Ying Shan, and Qifeng Chen. Fatezero: Fusing attentions for zero-shot text-based video editing. In *Proceedings of the IEEE/CVF International Conference on Computer Vision*, pages 15932–15942, 2023. 2

[32] Liao Qu, Huichao Zhang, Yiheng Liu, Xu Wang, Yi Jiang, Yiming Gao, Hu Ye, Daniel K Du, Zehuan Yuan, and Xinglong Wu. Tokenflow: Unified image tokenizer for multi-modal understanding and generation. In *Proceedings of the Computer Vision and Pattern Recognition Conference*, pages 2545–2555, 2025. 1, 2, 7

[33] Robin Rombach, Andreas Blattmann, Dominik Lorenz, Patrick Esser, and Björn Ommer. High-resolution image synthesis with latent diffusion models. In *Proceedings of the IEEE/CVF conference on computer vision and pattern recognition*, pages 10684–10695, 2022. 4

[34] Tiancheng Shen, Zilong Huang, Xiangtai Li, Zhijie Lin, Jiayang Liu, Yitong Wang, Jiashi Feng, Ming-Hsuan Yang, and Jun Hao Liew. Qk-edit: Revisiting attention-based injection in mm-dit for image and video editing. In *Proceedings of the IEEE/CVF International Conference on Computer Vision*, pages 19043–19053, 2025. 1, 2

[35] Uriel Singer, Amit Zohar, Yuval Kirstain, Shelly Sheynin, Adam Polyak, Devi Parikh, and Yaniv Taigman. Video editing via factorized diffusion distillation. In *European Conference on Computer Vision*, pages 450–466. Springer, 2024. 2, 5, 6, 7

[36] Wenhao Sun, Rong-Cheng Tu, Jingyi Liao, and Dacheng Tao. Diffusion model-based video editing: A survey. *arXiv preprint arXiv:2407.07111*, 2024. 1

[37] Hansi Teng, Hongyu Jia, Lei Sun, Lingzhi Li, Maolin Li, Mingqiu Tang, Shuai Han, Tianning Zhang, WQ Zhang, Weifeng Luo, et al. Magi-1: Autoregressive video generation at scale. *arXiv preprint arXiv:2505.13211*, 2025. 2

[38] Shuyuan Tu, Qi Dai, Zhi-Qi Cheng, Han Hu, Xintong Han, Zuxuan Wu, and Yu-Gang Jiang. Motioneditor: Editing video motion via content-aware diffusion. In *Proceedings of the IEEE/CVF Conference on Computer Vision and Pattern Recognition*, pages 7882–7891, 2024. 2

[39] Jing Wang, Fengzhuo Zhang, Xiaoli Li, Vincent YF Tan, Tianyu Pang, Chao Du, Aixin Sun, and Zhuoran Yang. Error analyses of auto-regressive video diffusion models: A unified framework. *arXiv preprint arXiv:2503.10704*, 2025. 5

[40] Wen Wang, Yan Jiang, Kangyang Xie, Zide Liu, Hao Chen, Yue Cao, Xinlong Wang, and Chunhua Shen. Zero-shot video editing using off-the-shelf image diffusion models. *arXiv preprint arXiv:2303.17599*, 2023. 2

[41] Yukun Wang, Longguang Wang, Zhiyuan Ma, Qibin Hu, Kai Xu, and Yulan Guo. Videodirector: Precise video editing via text-to-video models. In *Proceedings of the Computer Vision and Pattern Recognition Conference*, pages 2589–2598, 2025. 1, 2

[42] Ronald J Williams and David Zipser. A learning algorithm for continually running fully recurrent neural networks. *Neural computation*, 1(2):270–280, 1989. 4

[43] Bichen Wu, Ching-Yao Chuang, Xiaoyan Wang, Yichen Jia, Kapil Krishnakumar, Tong Xiao, Feng Liang, Licheng Yu, and Peter Vajda. Fairy: Fast parallelized instruction-guided video-to-video synthesis. In *Proceedings of the IEEE/CVF Conference on Computer Vision and Pattern Recognition*, pages 8261–8270, 2024. 1, 2, 6, 7

[44] Chenfei Wu, Jiahao Li, Jingren Zhou, Junyang Lin, Kaiyuan Gao, Kun Yan, Sheng-ming Yin, Shuai Bai, Xiao Xu, Yilei Chen, et al. Qwen-image technical report. *arXiv preprint arXiv:2508.02324*, 2025. 8

[45] Jay Zhangjie Wu, Yixiao Ge, Xintao Wang, Stan Weixian Lei, Yuchao Gu, Yufei Shi, Wynne Hsu, Ying Shan, Xiaohu Qie, and Mike Zheng Shou. Tune-a-video: One-shot tuning of image diffusion models for text-to-video generation. In *Proceedings of the IEEE/CVF international conference on computer vision*, pages 7623–7633, 2023. 2

[46] Jay Zhangjie Wu, Xiuyu Li, Difei Gao, Zhen Dong, Jinbin Bai, Aishani Singh, Xiaoyu Xiang, Youzeng Li, Zuwei Huang, Yuanxi Sun, et al. Cvpr 2023 text guided video editing competition. *arXiv preprint arXiv:2310.16003*, 2023. 5

[47] Zhen Xing, Qijun Feng, Haoran Chen, Qi Dai, Han Hu, Hang Xu, Zuxuan Wu, and Yu-Gang Jiang. A survey on video diffusion models. *ACM Computing Surveys*, 2023. 1

[48] Xiangpeng Yang, Linchao Zhu, Hehe Fan, and Yi Yang. Videograin: Modulating space-time attention for multi-grained video editing. In *The Thirteenth International Conference on Learning Representations*, 2025. 2

[49] Danah Yatim, Rafail Fridman, Omer Bar-Tal, Yoni Kasten, and Tali Dekel. Space-time diffusion features for zero-shot text-driven motion transfer. In *Proceedings of the IEEE/CVF Conference on Computer Vision and Pattern Recognition*, pages 8466–8476, 2024. 7

[50] Zixuan Ye, Huijuan Huang, Xintao Wang, Pengfei Wan, Di Zhang, and Wenhan Luo. Stylemaster: Stylize your video with artistic generation and translation. In *Proceedings of the Computer Vision and Pattern Recognition Conference*, pages 2630–2640, 2025. 2

[51] Tianwei Yin, Qiang Zhang, Richard Zhang, William T Freeman, Fredo Durand, Eli Shechtman, and Xun Huang. From slow bidirectional to fast autoregressive video diffusion models. In *Proceedings of the Computer Vision and Pattern Recognition Conference*, pages 22963–22974, 2025. 5

[52] Shoubin Yu, Difan Liu, Ziqiao Ma, Yicong Hong, Yang Zhou, Hao Tan, Joyce Chai, and Mohit Bansal. Veggie: Instructional editing and reasoning video concepts with grounded generation. In *Proceedings of the IEEE/CVF International Conference on Computer Vision*, pages 15147–15158, 2025. 1

[53] Hangjie Yuan, Weihua Chen, Jun Cen, Hu Yu, Jingyun Liang, Shuning Chang, Zhihui Lin, Tao Feng, Pengwei Liu, Jiazheng Xing, et al. Lumos-1: On autoregressive video generation from a unified model perspective. *arXiv preprint arXiv:2507.08801*, 2025. 2

[54] Zongsheng Yue, Jianyi Wang, and Chen Change Loy. Resshift: Efficient diffusion model for image super-resolution by residual shifting. *Advances in Neural Information Processing Systems*, 36:13294–13307, 2023. 3

[55] Chi Zhang, Chengjian Feng, Feng Yan, Qiming Zhang, Mingjin Zhang, Yujie Zhong, Jing Zhang, and Lin Ma. Instructvedit: A holistic approach for instructional video editing. *arXiv preprint arXiv:2503.17641*, 2025. 7

[56] Bojia Zi, Penghui Ruan, Marco Chen, Xianbiao Qi, Shaozhe Hao, Shihao Zhao, Youze Huang, Bin Liang, Rong Xiao, and Kam-Fai Wong. Señorita-2M: A high-quality instruction-based dataset for general video editing by video specialists. *arXiv preprint arXiv:2502.06734*, 2025. 2, 4, 5